Microelectronics Journal 40 (2009) 507–511

Contents lists available at ScienceDirect

Microelectronics Journal

journal homepage: www.elsevier.com/locate/mejo

Room temperature nano- and microstructure photon detectors

A.G.U. Perera [a,*], P.V.V. Jayaweera [a], G. Ariyawansa [a], S.G. Matsik [a], K. Tennakone [a], M. Buchanan [b], H.C. Liu [b], X.H. Su [c], P. Bhattacharya [c]

[a] Department of Physics and Astronomy, Georgia State University, Atlanta, GA 30303, USA
[b] Institute for Microstructural Sciences, National Research Council, Ottawa, Canada
[c] Solid State Electronics Laboratory, Department of Electrical Engineering and Computer Science, University of Michigan, Ann Arbor, MI 48109-2122, USA

ARTICLE INFO

Available online 21 July 2008

Keywords:
Infrared
Split-off band
PbS quantum dot
Tunneling quantum dot
Room temperature detector

ABSTRACT

The development of room temperature infrared (IR) detectors for wavelengths beyond NIR will open up many applications that are currently limited due to cooling requirements. Three approaches are discussed, which show promise for room temperature IR detection. Tunneling quantum dot (QD) detector, utilizes a tunneling barrier in order to block the dark current while permitting the photocurrent to pass through due to resonance effects, has shown room temperature response for a detector operating at 6 and 17 μm. The PbS QDs in a dielectric medium utilizes electronic polarizability of QDs, sensing only the variations of the radiation intensity, operating at ambient temperature. This method allows narrow multiple response bands. A GaAs/AlGaAs heterojunction detector, utilizing light, heavy and split-off hole transition in a *p*-doped semiconductor, shows a threshold of 3.4 μm operating up to 330 K.

1. Introduction

At present, commercially available infrared (IR) photon detectors work at cryogenic temperatures; thus, single element devices and focal plane arrays made of these detectors require cryogenic coolers. These detector systems are complicated, bulky, and also very expensive. The most effective way to overcome these drawbacks would be the development of IR detectors capable of operating at room temperature. The unique properties of low dimensional semiconductors offer opportunities for the application in almost all areas of electronics [1]. Many concepts have been extensively studied identifying potential applications. Quantum dots (QDs) are used in photon detection [2–5] especially the IR regions of the spectrum. Utilizing size quantized band-gap modulation, QDs of low effective carrier mass semiconductors, can be sensitized to the electromagnetic spectrum from ultraviolet to far IR. Here, we report three different techniques that show promising experimental results on room temperature IR photon detection.

2. Tunneling QD IR photodetector (T-QDIP)

In general, any device structure designed to reduce the dark current will also reduce the photocurrent. A new design, the T-QDIP can counteract this problem using resonant tunneling to selectively collect the photocurrent generated within the QDs, while the tunneling-barriers (double-barriers) block the majority of carriers contributing to the dark current, leading to high performances such as high responsivity, high detectivity, and high operating temperatures. A typical T-QDIP consists of InGaAs QDs embedded in a GaAs well, which is coupled to a AlGaAs/InGaAs/AlGaAs double-barrier. The conduction band profile of a T-QDIP structure under an applied bias is shown in Fig. 1(a). The photocurrent generated by a transition from a state in the QD (E_0, E_1, or E_2) to a state in the well (denoted as the resonant state, E_r, as this state is associated with resonance tunneling) which is coupled with a state in the double-barrier can be collected by resonant tunneling. The energy states in QDs are calculated using the 8-band **k.p** model [6]. Based on calculations, the allowed confined energy states in the QDs, E_0, E_1, and E_2 are located at −61, −103, and −73 meV with respect to the resonant state (see Fig. 1(a)). It can be shown that the tunneling probability is near unity for carriers excited by radiation with energy equal to the energy difference between the QD ground state (E_0) and the resonant state (E_r).

The structure of the T-QDIP grown by MBE is schematically shown in Fig. 1(b). Self-organized $In_{0.1}Ga_{0.9}As$ QDs were grown on a GaAs layer. A stack of $Al_{0.3}Ga_{0.7}As/In_{0.1}Ga_{0.9}As/Al_{0.3}Ga_{0.7}As$ layers serve as the double-barrier. The GaAs and AlGaAs layers were grown at 610 °C and the InGaAs or InAlAs QD layers were grown at 500 °C. Vertical circular mesas for top illumination were fabricated by standard photolithography, wet chemical etching and contact metallization techniques. The *n*-type top ring contact

* Corresponding author. Tel.: +1 404 413 6037; fax: +1 404 413 6025.
E-mail address: uperera@gsu.edu (A.G.U. Perera).

0026-2692/$ - see front matter © 2008 Elsevier Ltd. All rights reserved.
doi:10.1016/j.mejo.2008.06.019

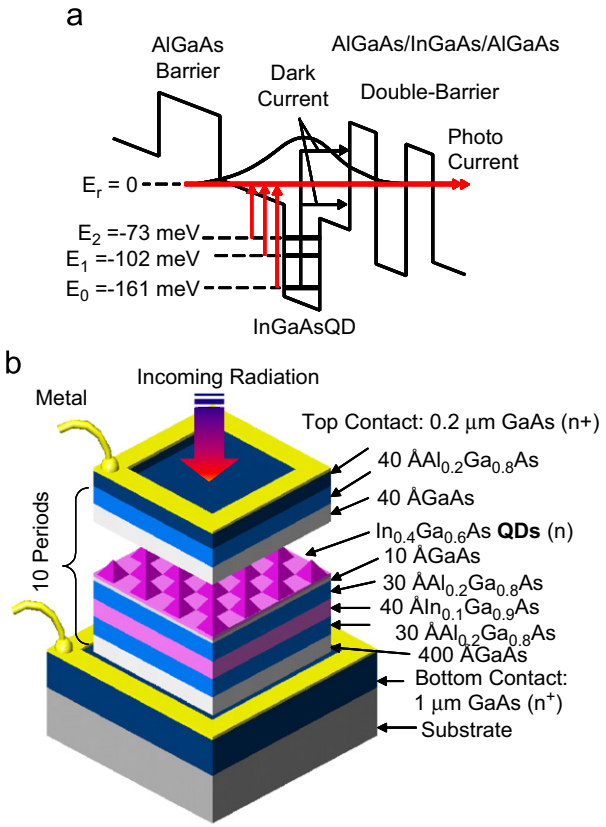

Fig. 1. (a) Conduction band profile of a T-QDIP structure under a bias. E_0, E_1, and E_2 are the energy level positions in the QD with respect to the resonant state E_r. The photocurrent generated by a transition from a state in the QD (E_0, E_1, and E_2) to the resonant state, E_r, which is coupled with a state in the double-barrier can be collected by resonant tunneling. (b) Schematic heterostructure of the T-QDIP grown by MBE. InGaAs QDs are placed in a GaAs well. The AlGaAs/InGaAs/AlGaAs layers serve as a double-barrier to decouple the dark and photo currents.

and the *n*-type bottom-contact were formed by evaporated Ni/Ge/Au/Ti/Au with a thickness of 250/325/650/200/2000 Å. The radius of the optically active area of the tested devices is 300 μm.

Dark current–voltage measurements were performed for both bias polarities, where positive (or negative) bias denotes positive (or negative) polarity on the top contact. Dark current densities at a bias of 1 V are 0.21, 0.96, and 1.55 A/cm^2 at 240, 280, and 300 K, respectively. These numbers are lower than other QDIPs [7] without double-barriers; hence, the reduction in the dark current of T-QDIP is associated with dark current blocking by the double-barrier. The spectral response of the T-QDIP under −2 V bias at different temperatures in the range of 200–300 K is shown in Fig. 2. Two distinct peaks centered around 6 and 17 μm were observed at high temperatures, and a weak response around 11 μm was also present. The peak at ~6 μm is due to transitions from the E_0 state to the E_r state, which is consistent with the calculated energy spacing ($\Delta E = 161$ meV). The peak at 17 μm results from transitions between the E_2 state to the E_r state ($\Delta E = 73$ meV). The line-width for this response is ~26 meV, which corresponds to the inhomogeneous broadening of QD states at 300 K. Due to the symmetry of QD geometry, excited states have a higher degeneracy (8) than the ground state (2). When the temperature is increased, the carrier density in excited states increases, as compared with that in the ground state. As a result, the 17 μm peak was dominant above 200 K, as evident from Fig. 2. The weak response at ~11 μm corresponds to the energy separation between the first excited QD state and the resonant state ($\Delta E = 102$ meV).

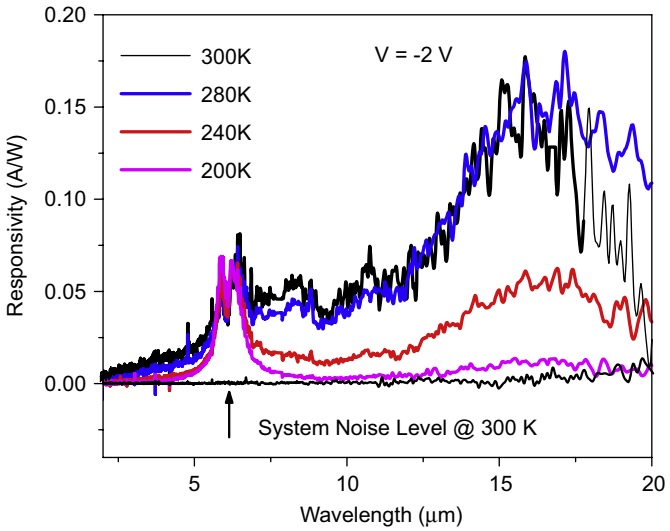

Fig. 2. Spectral responsivity of the T-QDIP in the temperature range 200–300 K under −2 V bias. Two distinct peaks centered around 6 and 17 μm can be observed at high temperatures, and a weak response around 11 μm is also visible. The system noise level at 300 K, which is a spectrum taken under dark conditions, is also shown.

The measured specific detectivity (D^*) at 17 μm and 300 K is of the order of 10^7 cm Hz$^{1/2}$/W, and with some re-designing of the device heterostructure, a higher detectivity is possible for the same operating conditions. While this demonstration of T-QDIP proves the feasibility of room temperature IR detector development, it also improves the understanding of underlying physics of QD-based devices, improving future device design and concepts. A T-QDIP in which QDs are coupled with two sets of double-barriers can be used to develop multi-band detectors with wavelength selectivity [8] with the applied bias. Furthermore, polarization sensitivity can be expected due to the dot-to-dot transitions. Hence, a T-QDIP would be a strong candidate for developing polarization sensitive multi-band detectors with a control capability of both spectral and polarization selectivity. Such detectors will be capable of capturing both the intensity and polarization contrast of the target.

3. QD capacitor-type photodetectors

Here, QDs are embeded in a film of high dielectric material to form a capacitor. The displacement current generated by modulated light incident on the dot/dielectric can be used as a signal to detect photons. As in pyroelectric detectors [9], this technique has the advantage that only the intensity modulated light generates signals enabling room temperature operation for sensing IR radiation. This is illustrated by designing a capacitor with PbS QDs embedded in paraffin wax as shown in Fig. 3(a).

Calculations indicate that QDs have several orders of magnitude larger polarizabilites than that of atoms and molecules [10]. This has been confirmed by the quantum confined stark effect [11,12] and measurement of the electronic polarizabilitiy of optically generated excitons in QD [13]. If a capacitor of thickness *s* consisting of *N* QDs of given size per unit volume is bias with *V* voltage current responsivity R_I (A/W) and voltage responsivity R_V (V/W) can be express as [14]

$$R_L = \frac{\sqrt{2}\phi(v)\omega V N \kappa \alpha \varepsilon_0}{hvs\sqrt{\omega^2 + k^2}} \quad (1)$$

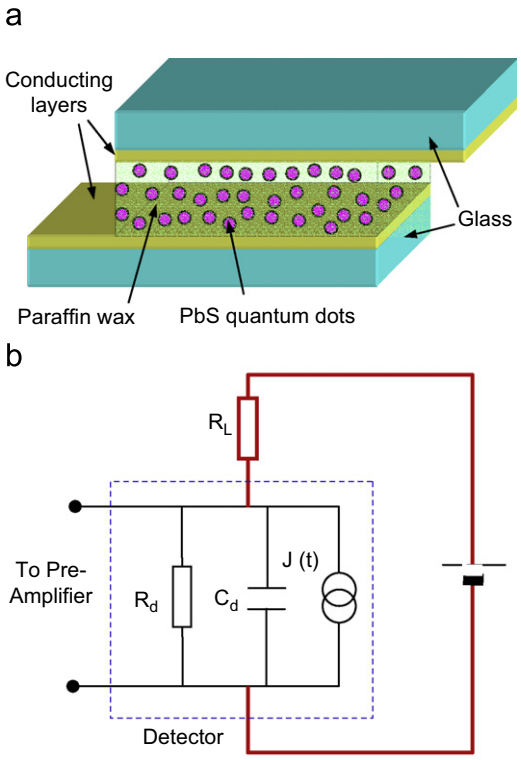

Fig. 3. (a) A schematics of the capacitive-type QD detector with PbS QD embedded in paraffin wax. The transparent conducting tin oxide (CTO)-coated glass plates were used as top and bottom contact. (b) The equivalent circuit of the detector and the circuit used for measurement of the photoresponse (C_d = detector capacitance, R_d = detector resistance).

$$R_V = \frac{\sqrt{2}\phi(v)\omega VN\kappa\alpha\varepsilon_0}{hvs\sqrt{\omega^2+k^2}} \times \frac{R_L \times R_d}{R_L + R_d} \quad (2)$$

where $\phi(\upsilon)$ is the quantum efficiency, ω the incident radiation chopping frequency, of exciton formation, and k the exciton recombination rate constant. α is the exciton polarizability, ε_0 the dielectric constant of the composite, υ the incident IR radiation frequency, h the plank constant, and R_L, R_d as indicated in Fig. 3(b). Detailed calculation can be found in Ref. [14].

The circuit used for the measurement of the photoresponse, including the equivalent circuit of the detector is shown in Fig. 3(b). The effect of the parasitic capacitance in the circuit is not very strong at low chopping frequencies (i.e., $\omega < [R_d C_d]^{1/2}$). A plot of responsivity vs. wavelength at different bias voltages (8.7–40 V) and a fixed chopping frequency of 57 Hz is shown in Fig. 4. The intrinsic responsivity of the detector can be calculated using Eq. (1) in terms of the properties of the QDs, the embedding dielectric medium, the thickness of the film, and the bias voltage. Responsivity depends on several factors, such as size and the number density of QDs, their polarizability, the thickness of the capacitor, and the applied bias. The response increases linearly with the applied bias according to Eq. (2) up to ~20 V and deviation from linearity is seen thereafter. A higher bias will also increase the noise and at bias values exceeding the field ionization threshold, the motion of dissociated electrons and holes will also contribute to the displacement current, causing deviation from the linear variation. The recombination rate constant k (in Eq. (1)) which is sensitive to the structure of the dot (i.e., capping, size, and shape) and its environment. For optimization of the responsivity, the QDs need to be densely packed, keeping the film thickness s comparable to the mean free path of photons.

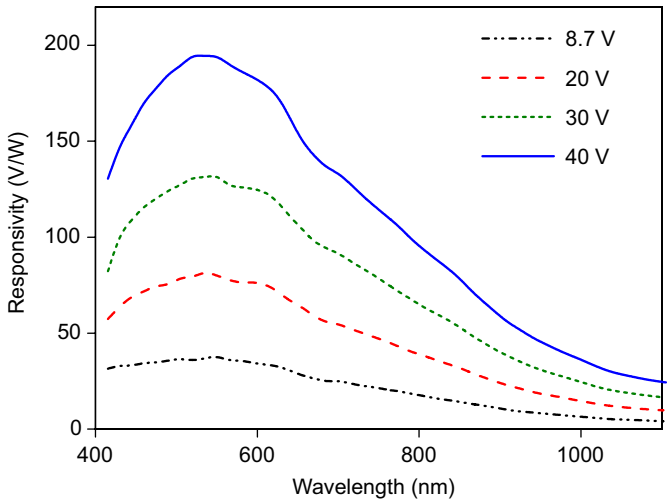

Fig. 4. The measured responsivity of the detector under different bias voltages (85 MΩ resistor was used as load resistor R_L and chopping frequency was 57 Hz).

However, in general conductor–insulator composites exhibit percolation thresholds [15] when the packing fraction of the conducting material exceeds a critical value N_C. When the total amount of PbS incorporated into the wax reached ~15% by weight, PbS begins aggregating masking the detection of this effect. Almost complete absorption of incident radiation avoiding any percolation threshold would be possible by increasing the film thickness. In general, near percolation thresholds, systems tend to be noisy [15] and therefore optimization should be achieved by keeping N well below N_C and appropriately adjusting s. The plot of voltage responsivity vs. the wavelength of the incident radiation under different bias voltages (1–40 V) with an 85 MΩ load resistor (R_L) is shown in Fig. 4. The responsivity at the peak absorption (λ = 540 nm) was found to be 195 V/W at a bias of 40 V and the specific detectivity under the same condition was determined as 3×10^8 cm Hz$^{1/2}$/W.

The responsivity of the present system can be compared with that of a photoconductive detector of the same bulk material as follows. As photoconductive current density is $J_c = en\mu E (\mu = e\tau/m$, μ = mobility, τ = scattering time, m = carrier effective mass and taking low-frequency molecular exciton polarizability $= e^2/\varepsilon_0 m\omega_0^2$ (ω_0 = exciton binding energy/h), we obtain $J/J_C = (\omega sNA/\tau\omega_0^2) \times 10^{-5}$ (A = detector area = 1 cm^2, ω = 57 Hz, $N = 10^7$, and exciton binding energy = 10 meV). The responsivity is low compared with a photoconductive detectors due to the less than ideal coverage of QDs in the dielectric (i.e., $N = 10^7$). Paraffin wax is not the best material to be used as the dielectric medium to embed QDs owing to its low melting point and brittleness. Here, we used paraffin wax due to the simplicity of the preparation but other dielectric material including silica, glass or polymers would be a better choice. It is straightforward to extend the proposed concept to QDs of other materials and nanowires. The effects of multi-exciton production will also be reminiscent in these detectors, especially if PbS is replaced by PbSe; In PbSe-conducting polymer photon detectors, enhancements in quantum efficiency originating from impact ionization has been observed [16]. Carbon nanotubes that possess high polarizabilities [17] with band gap taliorability would provide an option to fabricate multi-band detectors. Consequently, versatile photon detectors may be developed if nanotubes are used instead of QDs. An additional merit is the sensitivity to polarized radiation if the nanotubes are aligned in the dielectric medium. Furthermore, large aligning torques can be applied to carbon nanotubes, in a

highly resistive dielectric medium compared with a conducting medium.

4. Split-off band photon detectors

The split-off band effects have been experimentally observed in the emission of GaAs metal semiconductor field effect transistors [18] and have enhanced the response of GaInAsP [19] quantum wells. Extensive theoretical studies of the importance of the spin split-off band and the tunnelling properties of the holes through $Al_xGa_{1-x}As$/GaAs heterostructures is reported elsewhere [20]. Highly *p*-doped GaAs exhibits enhanced absorption around the 2–4 μm range due to split-off transitions. This can be utilized as an IR detection method for 2–4 μm range. The detection mechanism is based on intra-valance transitions of holes between the heavy/light hole bands and the spin split-off band. The active region of the detector consists of multiple periods of *p*-doped GaAs emitter and $Al_xGa_{1-x}As$ barrier regions sandwiched between two highly doped contact layers. A band diagram for a single period of a detector illustrating the different IR detection mechanisms is shown in Fig. 5. The internal workfunction Δ can be adjusted by varying the Al fraction x and the doping concentration of the emitter. The response can be due to four detection mechanisms, [21] as indicated by the arrows in Fig. 5. Three of them are associated with the split-off transitions and the fourth gives the free carrier mechanism [22]. Each mechanism consists of three processes: (a) photo-absorption that produces the excited carriers, (b) escape of the carriers, and (c) collection of the escaped carriers. Under equilibrium conditions, a *p*-doped emitter region will have a Fermi level in the light and heavy hole bands, but above the split-off band maximum. These transitions could be either direct or indirect transitions. Once the carrier is in the split-off band, it can escape directly or scatter back into the light/heavy hole bands and then escape. The wavelength threshold for mechanism (IV) will be shorter than for mechanisms (II) and (III) due to the requirement of passing the barrier in the split-off band. Based on the bandwidth and two thresholds in the experimental split-off response, both the direct and indirect absorptions are occurring in the split-off response. The large barriers required for high temperature operation will cause mechanisms (II) and (III) to be the dominant split-off response. Although mechanism (IV) is possible, its threshold will be near 1.5 μm.

A GaAs/$Al_xGa_{1-x}As$ detector with the Al fractions $x = 0.57$ (corresponding to Δ310 meV and threshold wavelength of 4 μm) was grown on a semi insulating GaAs substrate with a 0.7 μm thick bottom contact layer of $1 \times 10^{19}\,cm^{-3}$ *p*-doped GaAs followed by 30 periods of a 600 Å undoped $Al_xGa_{1-x}As$ barrier and $3 \times 10^{18}\,cm^{-3}$ *p*-doped 188 Å GaAs emitter. The last emitter was 0.2 μm thick and *p*-doped to $1 \times 10^{19}\,cm^{-3}$ in order to use as top contact layer. The detectors were processed by wet etching technique to form square mesas with sides of 400, 600, 800, and 1000 μm. Ti/Pt/Au ohmic contacts were evaporated onto the top and bottom contact layers. A ring contact was used on the top surface and a window was opened through the top contact for front side illumination. The schematic diagram is similar to Fig. 1(b) with 30 periods of p^+-GaAs emitter and $Al_xGa_{1-x}As$ barriers. The measured responsivity of the detector at 300 K under four different biases is shown in Fig. 6. The peak responsivity was 0.29 mA/W at 2.5 μm. Based on responsivity and the measured noise current density, peak detectivity (D^*) at 300 K was found to be as 6.8×10^5 Jones at 2.5 μm. As shown in Fig. 6, the responsivity increased with the bias, but increased dark current (low dynamic resistance) limited the maximum operating bias voltage to ~4 V. The threshold wavelengths for the different response mechanisms shown in Fig. 5 can be identified in Fig. 6. At 300 K process (II) becomes dominant, as can be seen by the much larger step at 2.9 μm than at 3.4 μm. The threshold for the free carrier response increased slowly with temperature due to the increased number of carriers above the Fermi energy, which can give rise to a response at longer wavelengths.

In conclusion, an uncooled IR detector based on a GaAs/AlGaAs multiple heterostructure responding up to 4 μm was reported. The response is primarily from heavy/light hole to split-off transitions and the detector shows a peak D^* of 6.8×10^5 Jones, at 2.5 μm and 300 K. As a well-developed material system, GaAs is one of the most feasible solution to the future uncooled IR detectors; since high-quality growth and integration into readout electronics will be readily available. Materials other than GaAs/AlGaAs may extend the response to longer wavelengths. Possible materials such as InP with a threshold of 11 μm and nitride materials may be able to operate up to 60 μm or beyond. Another possibility is to design a dual band detector that covers 3–5 and 8–14 μm

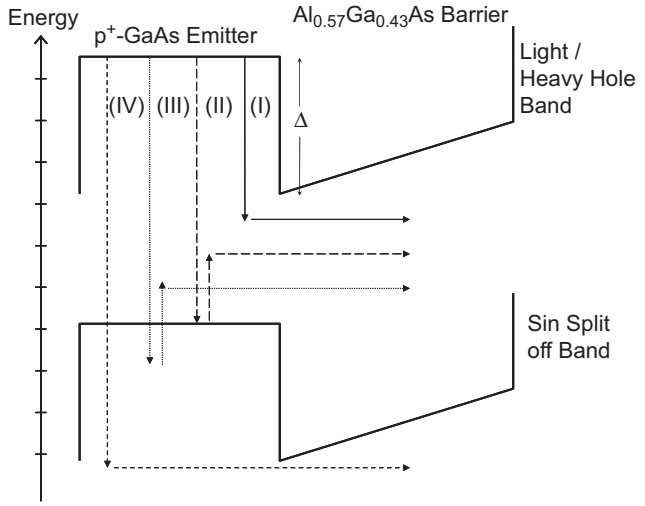

Fig. 5. A band diagram for a single period of a detector illustrating the four different IR detection mechanisms. Here, Δ is the workfunction for photoemission of carriers given by $\Delta = \Delta_d + \Delta_x$ where Δ_d and Δ_x are the contributions from the doping and the Al fraction, respectively.

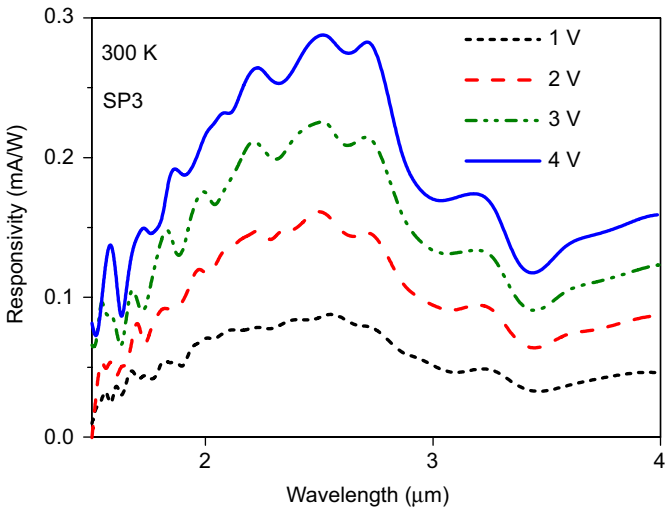

Fig. 6. The measured responsivity of the detector under four different biases at 300 K showing peaks around 2.5 μm.

atmospheric windows using a combined system with arsenide and phosphides.

Acknowledgments

This work was supported in part by the US NSF under Grants ECS-0553051, ECCS-0620688, INT-0322355, and OISE 0543257.

References

[1] A.D. Yoffe, Low-dimensional systems: quantum size effects and electronic properties of semiconductor microcrystallites (zero-dimensional systems) and some quasi-two-dimensional systems, Adv. Phys. 51 (2002) 799–890.
[2] D. Pal, J. Walker, E. Towe, InAs/GaAs quantum-dot infrared photodetectors grown by molecular beam epitaxy, J. Vac. Sci. Technol., B: Microelectron. Nanometer Struct. 24 (2006) 1532–1535.
[3] G. Konstantatos, I. Howard, A. Fischer, S. Hoogland, J. Clifford, E. Klem, et al., Ultrasensitive solution-cast quantum dot photodetectors, Nature 442 (2006) 180–183.
[4] H. Lim, S. Tsao, W. Zhang, M. Razeghi, High-performance InAs quantum-dot infrared photodetectors grown on InP substrate operating at room temperature, Appl. Phys. Lett. 90 (2007) 131112–131113.
[5] S. Krishna, S. Raghavan, G. Von Winckel, A. Stintz, G. Ariyawansa, S.G. Matsik, et al., Three-color ($\lambda_{p1}\sim$3.8, $\lambda_{p2}\sim$8.5 and $\lambda_{p3}\sim$23.2 μm) InAs/InGaAs quantum-dots-in-a-well detector, Appl. Phys. Lett. 83 (2003) 2745–2747.
[6] H. Jiang, J. Singh, Strain distribution and electronic spectra of InAs/GaAs self-assembled dots: an eight-band study, Phys. Rev. B 56 (1997) 4696–4701.
[7] G. Ariyawansa, A.G.U. Perera, G.S. Raghavan, G. Von Winckel, A. Stintz, S. Krishna, Effect of well width on three color quantum dots-in-a-well infrared detectors, IEEE Photon. Technol. Lett. 17 (2005) 1064.
[8] G. Ariyawansa, V. Apalkov, A.G.U. Perera, S.G. Matsik, G. Huang, P. Bhattacharya, Bias-selectable tricolor tunneling quantum dot infrared photodetector for atmospheric windows, Appl. Phys. Lett. 92 (2008) 111104-3.
[9] A. Hossain, M.H. Rashid, Pyroelectric detectors and their applications, IEEE Trans. Ind. Appl. 27 (1991) 824–829.
[10] F. Holka, P. Neogrády, V. Kellö, M. Urban, G.H.F. Diercksen, Polarizabilities of confined two-electron systems: the 2-electron quantum dot the hydrogen anion, the helium atom and the lithium cation, Mol. Phys. 103 (2005) 2747–2761.
[11] S.A. Empedocles, M.G. Bawendi, Quantum-confined stark effect in single CdSe nanocrystallite quantum dots, Science 278 (1997) 2114–2117.
[12] T. Unold, K. Mueller, C. Lienau, T. Elsaesser, A.D. Wieck, Optical stark effect in a quantum dot: ultrafast control of single exciton polarizations, Phys. Rev. Lett. 92 (2004) 157401–157404.
[13] F. Wang, J. Shan, M.A. Islam, I.P. Herman, M. Bonn, T.F. Heinz, Exciton polarizability in semiconductor nanocrystals, Nat. Mater. 5 (2006) 861–864.
[14] P.V.V. Jayaweera, A.G.U. Perera, K. Tennakone, Displacement currents in semiconductor quantum dots embedded dielectric media: a method for room temperature photon detection, Appl. Phys. Lett. 91 (2007) 063114-3.
[15] C.C. Chen, Y.C. Chou, Electrical-conductivity fluctuations near the percolation threshold, Phys. Rev. Lett. 54 (1985) 2529.
[16] D. Qi, M. Fischbein, M. Drndic, S. Selmic, Efficient polymer-nanocrystal quantum-dot photodetectors, Appl. Phys. Lett. 86 (2005) 093103-3.
[17] E.N. Brothers, G.E. Scuseria, K.N. Kudin, Longitudinal polarizability of carbon nanotubes, J. Phys. Chem. B 110 (2006) 12860–12864.
[18] K.S. Zhuravlev, V.A. Kolosanov, A.G. Milekhin, V.G. Polovinkin, T.S. Shamirzaev, N. Yu Rakov, et al., Infrared light emission from GaAs MESFETs operating at avalanche breakdown conditions, Semicond. Sci. Technol. 19 (2004) S94–S95.
[19] J.R. Hoff, M. Razeghi, G.J. Brown, Effect of the spin split-off band on optical absorption in p-type $Ga_{1-x}In_xAs_yP_{1-y}$ quantum-well infrared detectors, Phys. Rev. B 54 (1996) 10773–10783.
[20] S. Ekbote, M. Cahay, K. Roenker, Importance of the spin-orbit split-off band on the tunneling properties of holes through $Al_xGa_{1-x}As$/GaAs and InP/$In_yGa_{1-y}As$ heterostructures, Phys. Rev. B 58 (1998) 16315.
[21] A.G.U. Perera, S.G. Matsik, P.V.V. Jayaweera, K. Tennakone, H.C. Liu, M. Buchanan, et al., High operating temperature split-off band infrared detectors, Appl. Phys. Lett. 89 (2006) 131118-3.
[22] A.G.U. Perera, S.G. Matsik, B. Yaldiz, H.C. Liu, A. Shen, M. Gao, et al., Heterojunction wavelength-tailorable far-infrared photodetectors with response out to 70 μm, Appl. Phys. Lett. 78 (2001) 2241–2243.